Cuboid equivalent consumption minimization strategy for energy management of multi-mode plug-in hybrid vehicles considering diverse time scale objectives

Zhang, Cetengfei; Zhou, Quan; Hua, Min; Xu, Hongming; Bassett, Mike; Zhang, Fanggang

DOI:
10.1016/j.apenergy.2023.121901

Document Version
Publisher's PDF, also known as Version of record

Citation for published version (Harvard):
Zhang, C, Zhou, Q, Hua, M, Xu, H, Bassett, M & Zhang, F 2023, 'Cuboid equivalent consumption minimization strategy for energy management of multi-mode plug-in hybrid vehicles considering diverse time scale objectives', *Applied Energy*, vol. 351, pp. 121901. https://doi.org/10.1016/j.apenergy.2023.121901

Applied Energy 351 (2023) 121901

Contents lists available at ScienceDirect

Applied Energy

journal homepage: www.elsevier.com/locate/apenergy

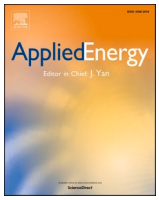

Cuboid equivalent consumption minimization strategy for energy management of multi-mode plug-in hybrid vehicles considering diverse time scale objectives

Cetengfei Zhang [a], Quan Zhou [a,*], Min Hua [a], Hongming Xu [a], Mike Bassett [b], Fanggang Zhang [a]

[a] Department of Mechanical Engineering, University of Birmingham, Birmingham B15 2TT, UK
[b] MAHLE Powertrain Ltd, Northampton, NN5 5TZ, UK

HIGHLIGHTS

- A cuboid equivalent consumption minimization strategy is proposed for PHEV
- Diverse time scale control objectives are incorporated into a new Hamilton matrix
- Pareto analysis is conducted to extract the optimal control settings
- 8.4% fuel and 10.4% battery capacity loss can be saved by the proposed method

ARTICLE INFO

Keywords:
Hybrid electric vehicles
Energy management
Multiple time scale optimization
Equivalent consumption minimization
Battery degredation

ABSTRACT

As a result of global actions for decarbonization, the rapid development of electrified vehicles (EV), including plug-in hybrid vehicles (PHEV) leads to increasing demands for maximizing battery useful life since recycling EV batteries would bring new environmental issues. PHEVs can have a higher fuel economy while maintaining the battery state-of-charge (SoC) through the equivalent consumption minimization strategy (ECMS); however, it is still a great challenge to maximize battery life through PHEV control since it is hard to balance diverse time scale control objectives (fuel economy, SoC control and the battery life). To this end, this paper proposes a Cuboid Equivalent Consumption Minimization Strategy (C-ECMS) for multimode PHEVs. A new concept of the "Hamiltonian matrix" is introduced by adding an additional control degree-of-freedom to the conventional Hamiltonian vector to enable optimal dual motor control in the multi-mode PHEVs. Then, an aging factor (AF) is introduced in associated with the equivalent factor (EF) to generate three Hamiltonian matrices that establish a cuboid knowledge base for the optimal control considering diverse time scale objectives. Experiments under five different driving cycles are conducted to study 1) the impact of Hamiltonian matrix dimensions on SoC control accuracy and 2) the impact of EF and AF settings on the Pareto Frontier considering fuel economy, SoC accuracy, and battery aging. The unified setting for C-ECMS is obtained based on the experimental study, and the result is demonstrated by a comparison study with the rule-based strategy and the standard ECMS implemented in the same PHEV. The results show that the proposed C-ECMS outperforms the standard ECMS control and achieves more accurate SoC sustaining (0.4% of SoC error), less fuel consumption (8.4% improvement), and less battery capacity loss (10.4% improvement).

1. Introduction

Electrified vehicles (EVs), including plug-in hybrid vehicles (PHEVs), are the key to decarbonization in the transport sector [1,2]. The energy management system (EMS) of PHEV is fatal to improve the vehicle's energy efficiency while maintaining the power units working in good conditions. Generally, the control functionalities of EMS are developed through rule-based methods (e.g., fuzzy logic [3]) or optimization-based methods [4,5]. Dynamic programming, genetic algorithm, and particle swarm optimization (PSO) [6,7] are developed for offline optimization

* Corresponding author.
E-mail address: q.zhou@bham.ac.uk (Q. Zhou).

https://doi.org/10.1016/j.apenergy.2023.121901
Received 12 June 2023; Received in revised form 7 August 2023; Accepted 2 September 2023
Available online 12 September 2023

of EMS. Online optimization methods, e.g., the equivalent consumption minimization strategy (ECMS) [4] and reinforcement learning [8], make PHEV more adaptive to real-world driving compared to the offline methods and are thus being widely studied.

Compared to RL, ECMS has relevant higher technical readiness and thus is under development by many automotive OEMs. During a driving process, the ECMS aims to minimize fuel and electrical power consumption simultaneously [9,10]. It dedicates the global optimization problem to a number of instant local optimization subproblems so that the PHEV can obtain the best control performance in the real-time control [11]. Because it does not need intricate training conditions, this technique is more computationally efficient than systems based on RL. The equivalent factor (EF), a weighting component in the Hamiltonian function that balances fuel and electricity use in the ECMS, substantially impacts the EMS's performance [12]. The value of EF will directly decide if the vehicle prefers thermal power (fuel consumption) and electrical power during the real-time driving process [13,14]. Generally, the decisive factors influencing EF adaption are road-related parameters (e.g., traffic conditions and terrain conditions [15–17]) and vehicle-related parameters (e.g., instant engine fuel consumption, battery states [18–20]).

Since the rapid increase in EV sales nowadays would lead to environmental issues when recycling the used EV batteries, maximizing the battery's useful life is becoming an essential task in the energy management control of EVs [21–23]. To evaluate battery degradation, battery state of health (SoH) is usually observed by monitoring battery impedance and capacity variation in the lab. Since it is impossible to measure the battery impedance in real-world driving, the battery capacity loss is usually estimated through the first principle modeling methods or data-driven methods [24] [25].

In the first principle model, the battery degradation is modeled based on internal electrochemical reactions with coupled multi-physics phenomena [26]. There are several software tools, e.g., COMSOL [27], that can simulate battery performance offline, but it is hard to implement these models for real-time control due to their high demands for computing resources [28,29]. The data-driven models are more computationally efficient in online control but require massive databases to train and validate the learning models [30,31]. In addition, it is hard to guarantee the robustness of the models since it is hard to consider all real-world scenarios in the R&D process [32,33]. Hence, there is a trend to develop battery degradation models by incorporating equivalent circuit models with empirical functions [34,35]. Wang et al. proposed an empirical degradation model considering C-rate, Ah-throughput, and battery temperature [36]. The model has been calibrated for many different applications including hybrid vehicles [37,38]. Therefore, this paper develops the battery model by incorporating Wang's empirical model into a 2RC equivalent circuit model, and the model parameters are calibrated with the data provided in [39] [40].

Since recycling batteries of electrified vehicles (EVs) would bring additional environmental problems, it is necessary to maximize battery usable battery life for EVs including PHEVs. Upgrading the standard ECMS with the capability to minimize battery degradation is an emerging topic in PHEV energy management [12]. There are several attends to introduce battery aging models in the ECMS for single-mode PHEVs, e.g., series PHEVs [16] and parallel PHEVs [19,41]. Liang et al. proposed a battery degradation considered ECMS based on a lookup table to control a multimode PHEV, but additional empirical rules are implemented to control the engine's working mode [42]. Sarvaiya et al. developed an ECMS based on the battery aging empirical equations for a parallel HEV [43]. Suri et al. developed the ECMS considering a battery severity map for a series HEV [35]. The main difference between single-mode PHEV and multi-mode PHEV is that the multi-mode PHEV has a coupling device, e.g., a clutch or a planetary gearset, to allow the PHEV to work in pure EV mode, series hybrid mode, or parallel mode. This allows more degree of freedom for power split for better fuel economy but brings challenges for designing ECMS because it needs to coordinate more control variables for optimal control.

In addition, multimode PHEV is more adaptive to real-world driving through mode switching, the multimode PHEV has tremendous potential for energy saving compared with the single-mode ones. However, the standard ECMS cannot be directly implemented for multiple mode energy management of the PHEV since the impact of the two motors on battery states cannot be fully considered in the conventional Hamiltonian function [8] [9]. Because battery aging is a long-term cumulative process and the EMS needs to balance the optimization objectives with various time scales, developing ECMS for multimode PHEVs is more complex [35]. To the best of the authors' knowledge, research is rarely done on ECMS considering multiple power sources based on diverse time scales.

To overcome the limitations of the existing ECMSs, this paper proposes a new Cuboid Equivalent Consumption Minimization Strategy (C-ECMS) for the multimode PHEV with two main contributions: 1) a new concept of "Hamiltonian matrix" is introduced by adding an additional control degree of freedom to the conventional Hamiltonian vector to enable optimal control of two motors in the multi-mode PHEVs; 2) an aging factor (AF) is introduced in associated with the equivalent factor (EF) to generate three Hamiltonian matrices that establish a cuboid knowledge base for the optimal control considering diverse time scale objectives. The unified setting for EF and AF is attained through a Pareto analysis of the impact of the EF and AF values on the vehicle energy efficiency, SoC control accuracy, and battery capacity loss.

The rest of this paper is organized as follows: Section 2 develops the models of the PHEV powertrain and the battery, and the optimization problem is formulated mathematically in Section 3. The C-ECMS is proposed in Section 4, and the results of the parametric study and the comparison study are presented in Section 5. Section 6 summarizes the conclusion.

2. PHEV powertrain and battery systems

This section introduces the specifications of the studied PHEV, where its powertrain architecture, key modeling parameters, and battery degradation are presented. The digital model of the powertrain and baseline strategies are sourced from MAHLE company in a format of MATLAB/Simulink, and it has been validated for practical usage.

2.1. Multi-mode PHEV powertrain

The architecture of the multi-mode PHEV powertrain is shown in Fig. 1. The main power units of this powertrain include a 70 kW internal combustion engine (ICE), two motor/generators (MG1 with a nominal power of 21 kW and MG2 with a nominal power of 135 kW) with integrated gearboxes, and a 20kWh battery. The dash green line illustrates the electric links, and the solid blue lines are mechanical links in the powertrain. At each instant time, the power requirement of the PHEV, P_{req}, and torque requirement of the PHEV, T_{req}, are

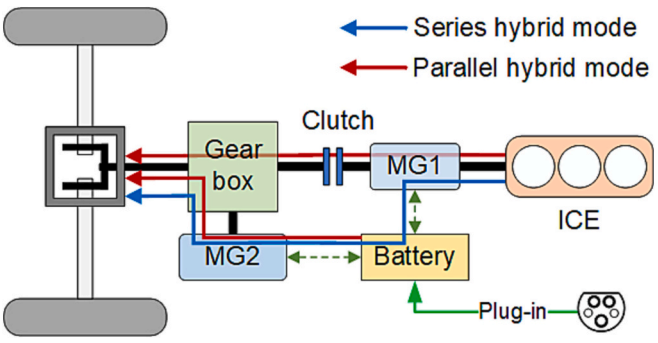

Fig. 1. The architecture of the PHEV

$$\left.\begin{aligned} P_{req} = F_{tot} \bullet v = \left(ma + C_f mg\, cos\theta + mg\, sin\theta + \frac{1}{2}\rho v^2 C_d A \right) \bullet v \\ T_{req} = F_{tot} \bullet R \end{aligned}\right\} \quad (1)$$

where F_{tot} is the total force demand by the vehicle; v is the vehicle speed; θ is the angle of the terrain slope; m is the vehicle mass; a is the acceleration of the vehicle; C_f is the rolling friction coefficient of the vehicle; g is the gravity acceleration; ρ is the air density; C_d is the aerodynamic drag coefficient, and A is the front area of the vehicle; T_{req} is the torque requirement at the wheel; R is the tire radius.

As illustrated in Fig. 1, the multi-model PHEV works in two operating modes, i.e., series mode (power flow shown in the blue arrow) and parallel mode (power flow shown in the red arrows). The mode switch is controlled through the clutch between the gear box and MG1. In the series mode, the clutch is disengaged, the MG2 solely drives the powertrain, and the range extender (ICE+MG1) works depending on the battery's state of charge (SoC). The energy flow of the PHEV in series mode yields

$$\left.\begin{aligned} P_{req} &= \eta_{MG2} P_{MG2} \\ T_{req} &= i_{RD} \bullet i_{R2} \bullet T_{MG2} \\ P_{Batt} &= \eta_{MG1} P_{MG1} \\ P_{ICE} &= P_{MG1} \\ \omega_{ICE} &= \omega_{MG1} \end{aligned}\right\} \quad (2)$$

where P_{ICE}, P_{Batt}, P_{MG2} and P_{MG1} are powers offered by the engine, battery, MG2 and MG1, respectively; η_{ICE}, η_{MG2} and η_{MG1}, are the corresponding efficiency of the engine, MG2 and MG1; T_{MG2} is the torque offered by MG2, and this torque is transmitted to the wheels through the gearbox integrated with MG2 (with the gear ratio i_{R2}) and the final differential (with the gear ratio i_{RD}); ω_{ICE} is the rotation speed of the engine, which is always the same as the rotation speed of MG1 (ω_{MG1}).

In the parallel mode, the ICE can provide part of the driving torque through the engaged clutch as compensation for the MG2. The energy flow of the PHEV in parallel mode yields

$$\left.\begin{aligned} P_{req} &= \eta_{MG2} P_{MG2} + (\eta_{ICE} P_{ICE} - P_{MG1}) \\ T_{req} &= i_{RD} \bullet i_{R2} \bullet T_{MG2} + i_{R1} \bullet (T_{ICE} - T_{MG1}) \\ P_{Batt} &= \eta_{MG1} P_{MG1} \\ \omega_{ICE} &= \omega_{MG1} \end{aligned}\right\} \quad (3)$$

where η_{ICE} is the engine efficiency; T_{ICE} and T_{MG1} are the torque outputs of the engine and MG1 respectively; i_{R1} is the transmission ratio of the gearbox to MG1.

A backward model is built in MATLAB/Simulink to simulate the power flow of the PHEV. The key parameters used for modeling are listed in Table 1.

Table 1
Specifications of the powertrain.

Component parameters	Values
Vehicle mass (m)	1700 kg
Tire rolling radius (R)	0.337 m
Rolling resistant coefficient (C_f)	0.011
Front Area (A)	2.5 m^2
Aerodynamic drag coefficient (C_d)	0.32
Engine displacement (D)	1 L
Battery capacity (C_{batt})	54.3 Ah
Battery nominal open-circuit-voltage (U_{OCV})	350 V
Differential ratio (i_{RD})	4.14
Transmission ratio of gearbox-MG1 (i_{R1})	0.95
Transmission ratio of gearbox-MG1 (i_{R2})	3.91

2.2. Battery equivalent circuit model and degradation model

To emulate the internal dynamics that affect battery aging, this paper builds a 2RC equivalent circuit battery model in MATLAB/Simulink as shown in Fig. 2.

The 2RC model determines battery current, I_{batt}, at every sampling time based on the powertrain power requirement, P_{batt}And the available battery voltage, U_t [44,45]. The governing equations of the 2RC model yields

$$\left.\begin{aligned} U_o &= I_{Batt} R_o \\ U_s &= \frac{I_{Batt}}{C_s} - \frac{U_s}{R_s C_s} \\ U_l &= \frac{I_{Batt}}{C_l} - \frac{U_l}{R_l C_l} \\ U_t &= U_{OCV} - U_s - U_l - U_o \end{aligned}\right\} \quad (4)$$

where U_o is the voltage drop caused by the Ohmic resistance; R_o is the battery Ohmic resistance; U_s represents the voltage drop in the charging transfer process; C_s and R_s are the short-term equivalent capacitance and resistance, respectively; U_l is the voltage indicating the battery diffusion process; C_l and R_l are long-term equivalent capacitance and equivalent resistance, respectively; and U_{OCV} is the open circle voltage, which is a function of the battery state of charge (SoC). The state-of-charge for the battery at the t-th time is calculated as.

$$SoC(t) = SoC(t_0) - \frac{\int_{t_0}^{t} I_{\text{Batt}}\, dt}{C_{\text{batt}}(t)} \quad (5)$$

where $SoC(t_0)$ denotes the initial SoC; $C_{\text{batt}}(t)$ denotes the battery's capacity; and I_{Batt} is the battery's current calculated from Eq.4.

Due to the difficulty of directly measuring the internal resistance, this paper mainly concentrates on the SoH degradation of the capacity loss. When the battery's capacity drops to a particular value (i.e., 20%), the battery is considered the end of life (EOL). From research by Wang et al. [36] and Song et al. [46], a semi-empirical model, with consideration of time, depth of charge (DoD), temperature and discharge rate, can be formulated mathematically as.

$$Q_{\text{Loss}} = Ae^{-\left(\frac{E_a + B \bullet C_{\text{Rate}}}{R_g T_{\text{batt}}}\right)} A_h{}^z \quad (6)$$

where Q_{Loss} is the capacity loss of battery; A is a pre-exponential factor; E_a is the activation energy; R_g is the gas constant; T_{batt} is the battery's absolute temperature; C_{Rate} is the C-rate of discharging; B is the compensation factor for the C-rate; $A = 0.0032$, $E_a = 15162$, $B = 1516$, and $z = 0.824$ are calibrated in work conducted by Song et al. [47,48]; A_h is the Ah-throughput; z is the power-law factor. This empirical model will later be applied with the battery's 2RC model to have a real-time reaction in the simulation for the PHEV.

The Ah-throughput, A_h, and the C-rate, C_{Rate}, can be calculated by.

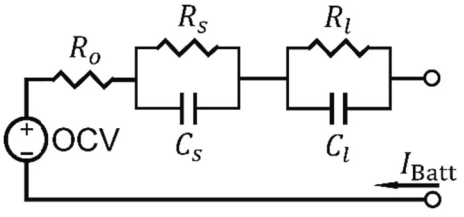

Fig. 2. The 2 RC battery model.

$$\left.\begin{aligned} A_h &= \frac{1}{3600}\int_{t_k}^{t_{k+1}} |I_{\text{batt}}|dt \\ \text{C}_{\text{Rate}} &= \frac{I_{\text{batt}}}{C_{\text{batt}}} \end{aligned}\right\} \tag{7}$$

where A_h is the Ah-throughput of the current integration of I_{batt} during the time t_k to t_{k+1}.

3. Energy management problem statement

The multi-objective optimization problem for the multi-mode PHEV considering fuel consumption,Q_{Fuel}, battery SoC control error, Q_{SoC}, and battery capacity loss, $Q_{\text{Loss}}(t)$, is formulated mathematically by

$$\{P_{ICE}(t), P_{MG1}(t), P_{MG2}(t)\} = argmin(Q_{Fuel}, Q_{SoC}, Q_{Loss}), t = 0, \ldots, T$$
$$s.t. \left\{\begin{array}{c} Equantions\ (1)-(5) \\ SoC_{min} \le SoC(t) \le SoC_{max} \\ 0 \le P_{ICE}(t) \le P_{ICEmax} \\ 0 \le P_{MG1}(t) \le P_{MG1max} \\ P_{MG2min} \le P_{MG2}(t) \le P_{MG2max} \end{array}\right\} \tag{8}$$

where SoC_{min} and SoC_{max} are the lower and upper boundaries of the battery SoC level; the power outputs of the engine ($P_{\text{ICE}}(t)$), the motor 1 ($P_{\text{MG1}}(t)$), and the motor 2 ($P_{\text{MG2}}(t)$) are limited by their constraints, and Q_{Loss} is the battery capacity loss defined by Eq.6. Moreover, the concentration is on the charging-sustaining (CS) process for this PHEV since it acts as a pure EV in charging-depleting (CD) driving process. Thus, the battery SoC of the PHEV at the end of driving is desired as the same as the initial value, by this end, energy variations can be indicated only based on the fuel consumption.

The energy consumption over the driving, Q_{Fuel}, is calculated by

$$Q_{Fuel} = \int_0^T \dot{m}_{ICE}(T_{ICE}(t), \omega_{ICE}(t))\, H_{LHV}\, dt \tag{9}$$

where T is the overall driving time; $\dot{m}_{\text{ICE}}$ represents the instant fuel flow rate at the t – th step, which depends on a fuel mass flow rate map of engine speed, ω_{ICE} and engine torque T_{ICE}; and H_{LHV} represents the lower heating value of the fuel, which is usually 43.4 MJ/kg for gasoline [49].

The relative SoC error Q_{SoC} is defined as

$$Q_{\text{SoC}} = \left|\frac{SoC_{\text{final}} - SoC_{\text{target}}}{SoC_{\text{target}}}\right| \tag{10}$$

where SoC_{final} is the SoC level at the end of the driving; and SoC_{target} is the target SoC level.

In this paper, SoC_{target} is set to 0.3 because it is a widely accepted value for PHEV control concerning battery operation safety [40,41].

4. Cuboid equivalent consumption minimization strategy

This section develops the cuboid equivalent consumption minimization strategy (C-ECMS) based on standard ECMS. First, the mechanism of the standard ECMS is introduced in section 4.1. Then, in section 4.2, the C-ECMS is proposed by upgrading the conventional Hamiltonian vector into a Hamiltonian matrix for optimal control of the multimode PHEV, as illustrated in Fig. 3. In section 4.3, the online application of the C-ECMS is demonstrated. Based on the battery degradation model developed in section 2.2, the aging factor (AF) is introduced to work jointly with the equivalent factor (EF) to generate three Hamiltonian matrices that form a cuboid knowledge base for energy management of the multimode PHEV.

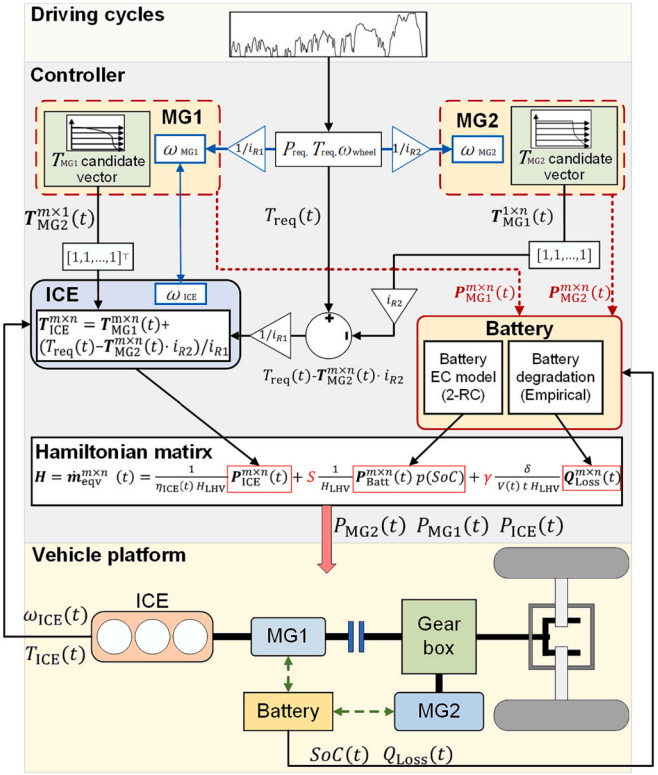

Fig. 3. The architecture of C-ECMS.

4.1. The standard ECMS

The core idea of ECMS is that the electrical energy can be approximately converted to fuel consumption based on the Hamiltonian function that is centered around an equivalent factor (EF) [12]. The Hamiltonian function value can be calculated by

$$\left.\begin{aligned} H(t) &= \dot{m}_{eqv}(t) = \dot{m}_{ICE}(t) + \dot{m}_{Batt}(t) \\ \dot{m}_{ICE}(t) &= \frac{P_{ICE}(t)}{\eta_{ICE}(t)\, H_{LHV}} \\ \dot{m}_{Batt}(\text{t}) &= \frac{S}{H_{LHV}} P_{Batt}(t) \end{aligned}\right\} \tag{11}$$

where $\dot{m}_{\text{eqv}}(t)$ is the instant equivalent consumption (EC) of fuel at the t-th time step; $\dot{m}_{\text{batt}}(t)$ represents the equivalent fuel consumption from the electrical energy; S is the equivalent factor (EF), which needs to be calibrated for different driving cycles; and H_{LHV} is the lower heating value of the fuel.

The candidate power offered by the battery can be discretized with finite numbers, and a candidate vector with a set of indices, $\vec{n} = [0, 1, 2, 3 \ldots (n-1)]$, is used to generate a vector of battery candidate power values as

$$\vec{P}_{Batt}(t) = P_{Batt,min}(t) + \vec{n} \times \frac{[P_{Batt,max}(t) - P_{Batt,min}(t)]}{n} \tag{12}$$

where $P_{\text{Batt},min}(t)$ and $P_{\text{Batt},max}(t)$ are the lower and upper limits of the battery potential power output at the t-th time, respectively.

Since only a motor is considered in the standard ECMS, the vector of the candidate ICE power values, $\vec{P}_{ICE}$, and the vector of candidate MG power values, $\vec{P}_{MG}$, can be calculated by

$$\left.\begin{aligned} \vec{P}_{ICE}(t) &= P_{req}(t) - \vec{P}_{Batt}(t) \\ \vec{P}_{MG}(t) &= \vec{P}_{Batt}(t) \end{aligned}\right\} \tag{13}$$

By incorporating Eqs. 11–13, the Hamiltonian vector can be obtained at each instant time as

$$\overrightarrow{H} = \frac{\overrightarrow{P}_{ICE}}{\eta_{ICE}(t)\, H_{LHV}} + \frac{S}{H_{LHV}} \overrightarrow{P}_{Batt} \bullet p(SoC) \tag{14}$$

where $p(SoC)$ is a penalty function to control the SoC level during the control process [11]. Its formulation is expressed as

$$p(SoC) = 1 - \left(\frac{SoC(\mathrm{t}) - SoC_{\mathrm{target}}}{SoC_{\max} - SoC_{\min}} \right)^{\alpha} \tag{15}$$

where $SoC(\mathrm{t})$ is the SoC level of the battery, $SoC_{\max}$ and $SoC_{\min}$ are the operational range limits of the battery during the driving process, respectively. In this paper, $SoC_{\max}$ =0.8, $SoC_{\min}$ =0.2 and α =3, which are widely accepted values for PHEV control [51].

At each sampling time, the ECMS will find an index value, opt $\in [1, n]$, that satisfies

$$\overrightarrow{H}(\mathrm{opt}) \le \overrightarrow{H}(j), i \in [1, n] \tag{16}$$

and will output the values of $\overrightarrow{P}_{\mathrm{Batt}}(\mathrm{opt})$, $\overrightarrow{P}_{\mathrm{MG}}(\mathrm{opt})$, and $\overrightarrow{P}_{\mathrm{ICE}}(\mathrm{opt})$ for real-time control.

4.2. The Hamiltonian matrices for multiple motors

To enable dual-motor controls in the multimode PHEV, two torque candidate vectors are established for MG1 and MG2 by introducing two index vectors, $\overrightarrow{n} = [0, 1, 2, 3, \ldots, n-1]$ and $\overrightarrow{m} = [0, 1, 2, 3, \ldots, m-1]^{\top}$,

$$\left.\begin{aligned} \boldsymbol{T}_{\mathrm{MG1}}^{1\times n}(t) &= T_{\mathrm{MG1},min}(t) + \overrightarrow{n} \times \frac{\left[T_{\mathrm{MG1},max}(t) - T_{\mathrm{MG1},min}(t)\right]}{n} \\ \boldsymbol{T}_{\mathrm{MG2}}^{m\times 1}(t) &= T_{\mathrm{MG2},min}(t) + \overrightarrow{m} \times \frac{\left[T_{\mathrm{MG2},max}(t) - T_{\mathrm{MG2},min}(t)\right]}{m} \end{aligned}\right\} \tag{17}$$

where $\boldsymbol{T}_{\mathrm{MG1}}^{1\times n}(t)$and $\boldsymbol{T}_{\mathrm{MG2}}^{m\times 1}(t)$ are the torque candidate vectors of the MG1 and MG2.

Two power matrices are introduced for the candidate power of MG1 and MG2 at time t as follows

$$\left.\begin{aligned} \boldsymbol{P}_{\mathrm{MG1}}^{m\times n}(t) &= \frac{\omega_{\mathrm{wheel}}(t)}{i_{R1} \bullet i_{RD}} \bullet \left[\underbrace{1, 1, \ldots, 1}_{m}\right]^{\top} \times \boldsymbol{T}_{\mathrm{MG1}}^{1\times n}(t) \\ \boldsymbol{P}_{\mathrm{MG2}}^{m\times n}(t) &= \frac{\omega_{\mathrm{wheel}}(t)}{i_{R2} \bullet i_{RD}} \bullet \boldsymbol{T}_{\mathrm{MG2}}^{m\times 1}(t) \times \left[\underbrace{1, 1, \ldots, 1}_{n}\right] \end{aligned}\right\} \tag{18}$$

The potential power offered by the battery is calculated by

$$\boldsymbol{P}_{\mathrm{Batt}}^{m\times n}(t) = \boldsymbol{P}_{\mathrm{MG1}}^{m\times n}(t) + \boldsymbol{P}_{\mathrm{MG2}}^{m\times n}(t) \tag{19}$$

The ICE compensates for the power gap between the instant power requirement and the power offered by the battery. Mathematically, it is presented as.

$$\boldsymbol{P}_{\mathrm{ICE}}^{m\times n}(t) = P_{\mathrm{req}}(t) - \boldsymbol{P}_{\mathrm{Batt}}^{m\times n}(t) \tag{20}$$

Based on Eqs. 17–20, the Hamiltonian matrix is formulated as.

$$\boldsymbol{H}_{\mathrm{mtx}}^{m\times n}(t) = \dot{\boldsymbol{m}}_{\mathrm{eqv}}^{m\times n}(t) = \frac{1}{\eta_{\mathrm{ICE}}(t)\, H_{\mathrm{LHV}}} \boldsymbol{P}_{\mathrm{ICE}}^{m\times n}(t) + \frac{S}{H_{\mathrm{LHV}}} \boldsymbol{P}_{\mathrm{Batt}}^{m\times n}(t) \bullet p(SoC) \tag{21}$$

4.3. Cuboid knowledge base for energy management

Based on Eqs. 5–7, two matrices for battery capacity loss, $\boldsymbol{Q}_{\mathrm{Loss}}^{m\times n}$, and the Ah-throughput, $\boldsymbol{A}\boldsymbol{h}_{\mathrm{Batt}}^{m\times n}$, can be formulated as.

$$\left.\begin{aligned} \boldsymbol{A}\boldsymbol{h}_{\mathrm{Batt}}^{m\times n} &= \frac{1}{3600} \int_{t_k}^{t_{k+1}} \left| \frac{\boldsymbol{P}_{\mathrm{Batt}}^{m\times n}(t)}{U(t)} \right| dt \\ \boldsymbol{Q}_{\mathrm{Loss}}^{m\times n} &= A\, exp\left(- \left(\frac{E_a + B \bullet \dfrac{\boldsymbol{I}_{\mathrm{Batt}}^{m\times n}(t)}{C_{\mathrm{batt}}}}{R_g T_{\mathrm{batt}}} \right) \right) \left(\boldsymbol{A}\boldsymbol{h}_{\mathrm{Batt}}^{m\times n}\right)^{z} \end{aligned}\right\} \tag{22}$$

By combining Eq.21 and Eq.22, the cuboid knowledge base, as illustrated in Fig. 4 is formulated by the Hamiltonian matrix.

$$H(t) = \underbrace{\frac{1}{\eta_{\mathrm{ICE}}(t) H_{\mathrm{LHV}}} \boldsymbol{P}_{\mathrm{ICE}}^{m\times n}(t)}_{\text{Actual consumption by ICE}} + \underbrace{\frac{S}{H_{\mathrm{LHV}}} \boldsymbol{P}_{\mathrm{Batt}}^{m\times n}(t) \bullet p(SoC)}_{\text{EC by battery}} + \underbrace{\gamma \frac{\delta}{U(t)\, t H_{\mathrm{LHV}}} \boldsymbol{Q}_{\mathrm{Loss}}^{m\times n}(t-1, t)}_{\text{battery capacity loss penalty}} \tag{23}$$

where the first item on the right-hand side is the actual fuel consumption by the ICE. The second item is the equivalent fuel consumption by the battery. The third item is the penalty of equivalent fuel consumption caused by the capacity loss (the capacity loss Ah is transferred into fuel flow rate); γ is an aging factor; and δ is a gain factor to unify the magnitude of battery capacity loss with the other components. In this paper, $\delta = 10^6$, according to the magnitude of values in the Hamiltonian function of C-ECMS.

For the C-ECMS, a cuboid knowledge base is established by calculating the total Hamiltonian values based on Eq.23 for different combinations of clutch state (determining the operating mode) and the power outputs of MG1, MG2, and ICE, as illustrated in Fig. 4. From the cuboid knowledge base, an indicator with the minimum EC value can be retrieved in each control time step based on the power demand of the multi-mode PHEV. With the indicator, the clutch state and the power outputs of MG1, MG2, and ICE can be found for real-time control.

5. Results and discussions

Experiments under five driving cycles are conducted to study 1) the impact of the number of elements in Hamiltonian matrices on SoC control accuracy and 2) the impact of EF and AF settings on the Pareto Frontier considering fuel economy, SoC accuracy, and battery aging. WLTP3, Artemis Urban, Artemis Rural Road, Artemis Motorway 130, and RTS95 driving cycles were chosen for the study to over the most driving conditions of the PHEV. WLTP3 contains comprehensive driving scenarios of PHEVs with low, medium, and high-speed ranges, the Artemis series diving cycles can represent the most real-world driving conditions with transient speed variations, while the RTS95 cycle represents the aggressive driving styles. Table 2 summarized the general information about the five driving cycles. Based on the experimental study, the unified setting for C-ECMS is obtained, and the result is validated by a comparison study with the rule-based strategy and the standard ECMS implemented in the same PHEV.

5.1. Impact of number of elements in the Hamiltonian matrices on SoC control accuracy

The number of elements in the Hamiltonian matrices affects the information stored in the knowledge base for MG1 and MG2 control. Theoretically, more information in the Hamiltonian matrix will result in more accurate control performance (i.e., less SoC control error) but require more computational resources. Thus, the values of n and m that determine the size of Hamiltonian matrices need to be set appropriately. The values of n and m lies in their critical role in achieving an optimal energy distribution between the motors (MG1 and MG2) and the engine (ICE) during the control process. By selecting these parameters, we can effectively balance the power allocation among the different components of the powertrain, leading to improved energy efficiency and reduced fuel consumption. To attain the optimal setting of n and m, this

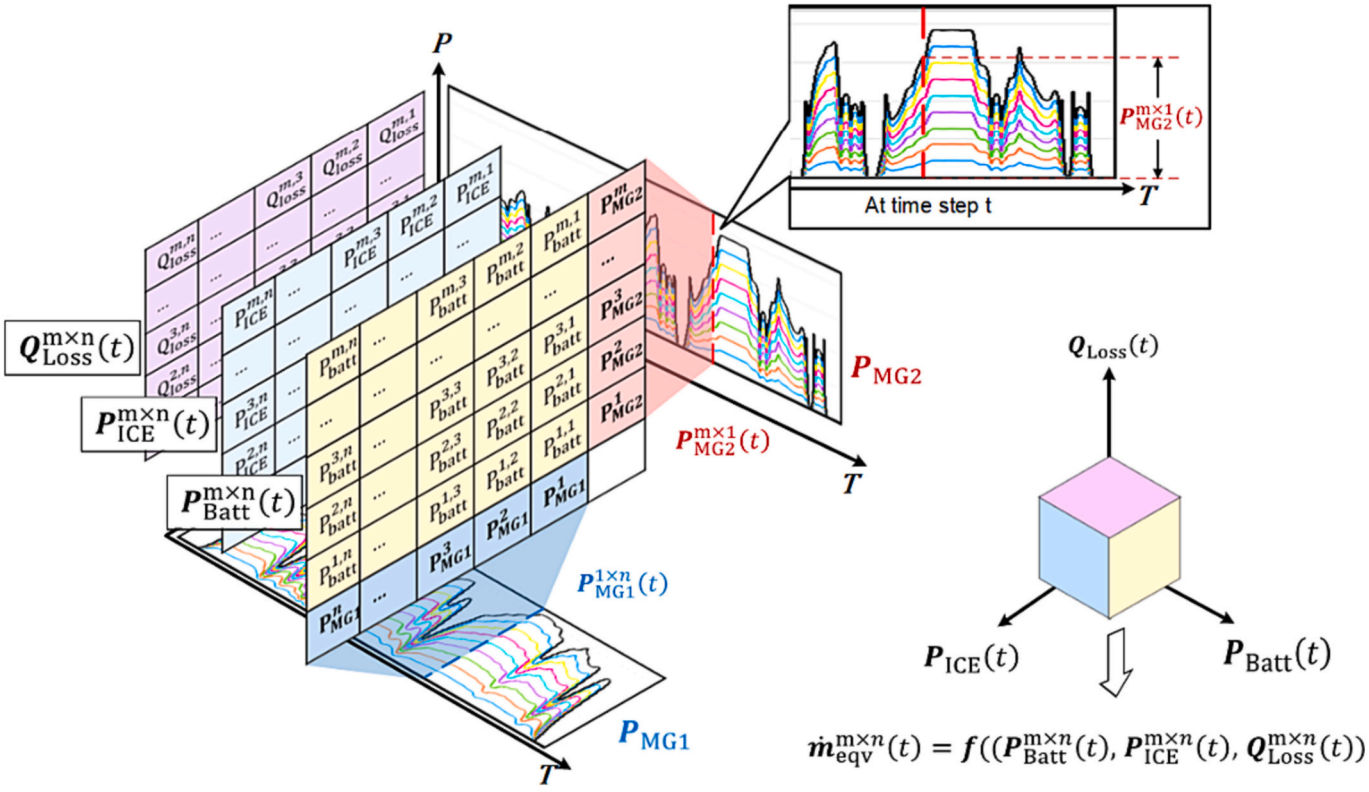

Fig. 4. The cuboid knowledge base for C-ECMS.

Table 2
Information about the driving cycles.

Driving cycles	Features	Single cycle duration (s)	Maximum speed (km/h)	Average speed (km/h)
WLTP3	Urban, suburban, rural and highway scenarios	1800	131.3	46.5
Artemis Urban	Urban scenarios	993	57.3	17.7
Artemis Rural Road	Rural road scenarios	1082	111.1	57.5
Artemis Motorway 130	Motorway scenarios	1068	131.4	96.9
RTS95	aggressive driving in urban, rural and motorway scenarios	886	134.5	52.5

paper optimizes the following mathematical problem

$$\left.\begin{aligned} \{n,m\} &= argmin(Q_{SoC}) \\ Q_{SoC} &= \left|\frac{SoC_{final} - SoC_{target}}{SoC_{target}}\right| \times 100\% \\ s.t. n,m &\in \mathbb{Z}^+ \end{aligned}\right\} \tag{24}$$

where n and m define the number of elements for power distributions of MG1 and MG2, respectively; Q_{SoC} is the relative error between the final SoC by the end of the driving cycle (SoC_{final}) and the target SoC ($SoC_{target} = 0.3$, in this paper).

The relative errors of battery SoC are obtained by different combinations of the number of elements in the Hamiltonian matrices in Fig. 5. The colored lines in Fig. 5 are contours representing the SoC error levels

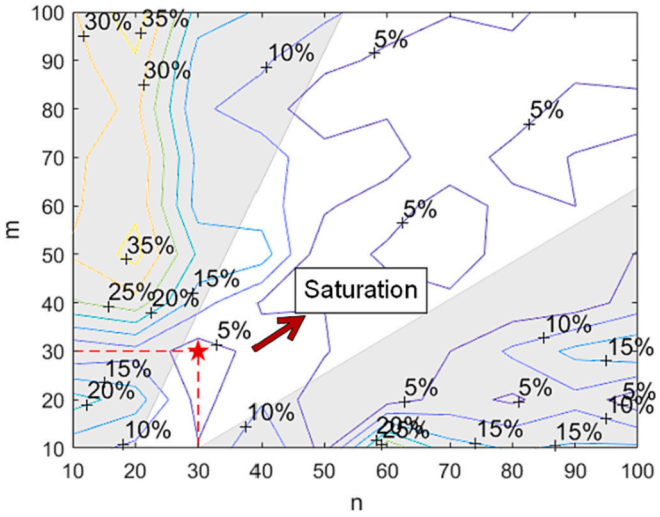

Fig. 5. The numerical analysis of power discretization.

achieved by different sizes of Hamiltonian matrices that were determined by n and m. The contour's display is set with a minimum level of 5% to distinguish the errors' distribution. The minimum number of elements in the Hamiltonian matrices is set as 10 since the power discretization below such a limit is severely harsh for the calculation. The maximum number of elements is set as 100 based on the instant power matrices calculation limitation in time seconds. Also, in Fig. 5, the 'saturation' represents that when the combination of n and m continues to increase along the direction of the arrow (in the white region that is not covered by the shadow), the SoC error will no longer decrease further. At this stage, the computational accuracy has reached saturation. Fig. 5 indicates that when $n = 30$ and $m = 30$, the C-ECMS can

achieve its best performance in SoC sustaining leading to the minimum SoC error of less than 5%. Fig. 5 also highlights that when the values of n and m are not selected properly, e.g., in the grey area, the C-ECMS cannot guarantee a stable control of battery SoC, i.e., SoC error is higher than 10%.

5.2. Impact of the equivalent factor and the aging factor on control performances

The proposed C-ECMS introduced an additional aging factor (AF) to resolve the multi-objective optimization problem in real-time control, therefore, the impact of the values of AF and EF factors on the control performances are investigated in this section. Firstly, we design an orthogonal experiment to generate 5600 sample points for C-ECMS with different AF and EF settings, where the AF values are set from 0 to 2 with an interval size of 0.025 and the EF values are set from 0.5 to 4 with an interval size of 0.05. Then, we implemented the 5600 groups of settings into the studied multi-mode PHEV and examined its performance (concerning fuel economy, SoC sustaining error, and battery capacity loss) under five driving cycles including WLTP3, Artemis-Urban, Artemis-Rural Road, Artemis-Motorway 130, and RTS95. Based on the 5 × 5600 groups of results obtained under the five driving cycles, we obtained five Pareto Frontiers (PFs) by applying the principle of Pareto domination, which is defined as follows,

$$P(\boldsymbol{Y}) = \{\boldsymbol{y}^{'} \in \boldsymbol{Y} : \{\boldsymbol{y}^{''} \in \boldsymbol{Y} : \boldsymbol{y}^{''} \succ \boldsymbol{y}^{'}, \boldsymbol{y}^{''} = \boldsymbol{y}^{'}\} = \varnothing\} \tag{25}$$

where $P(\boldsymbol{Y})$ is the solutions on the PF; $\boldsymbol{Y}$ is the feasible set of objective functions in $\mathbb{R}^3$, such that $\boldsymbol{Y} = \left\{\boldsymbol{y} = [Q_{Fuel}, Q_{Loss}, Q_{SoC}]^T \in \mathbb{R}^3 : [Q_{Fuel}, Q_{Loss}, Q_{SoC}]^T = \mathscr{M}(AF, EF, DC)\right\}$; $\boldsymbol{y}^{''} \succ \boldsymbol{y}^{'}$ denotes that the values of all the elements in the vector $\boldsymbol{y}^{''}$ dominate the values of enlacements in $\boldsymbol{y}^{'}$; and $\mathscr{M}$ is the PHEV model running with different AF and EF values under a given driving condition, DC.

Five Pareto frontiers (PFs) obtained with different AF and EF values under five standard cycles are shown in Fig. 6, where the PFs are visualized in a 3D space and projected into the 2D planes for analysis. Fig. 6 (b), (c), and (d) present the relationships between any two of the three optimization objectives, i.e., the fuel economy, the final SoC error, and the battery capacity loss. As shown in Fig. 6 (c), battery capacity loss and fuel economy have a clear trade-off relationship, which means when more battery capacity loss needs to be reduced the fuel economy needs to be sacrificed. According to Fig. 6 (b), for most cases (4 out of studied 5 driving cycles), the battery capacity loss is not linear correlated to the SoC sustain error, which means that we cannot always mitigate the battery capacity loss by minimizing the SoC sustaining errors. Fig. 6 (c) also shows that the fuel economy and SoC sustaining error has no strong correlation. Therefore, the proposed 3D Hamiltonian matrix is necessary since we cannot simply incorporate the task for battery capacity loss

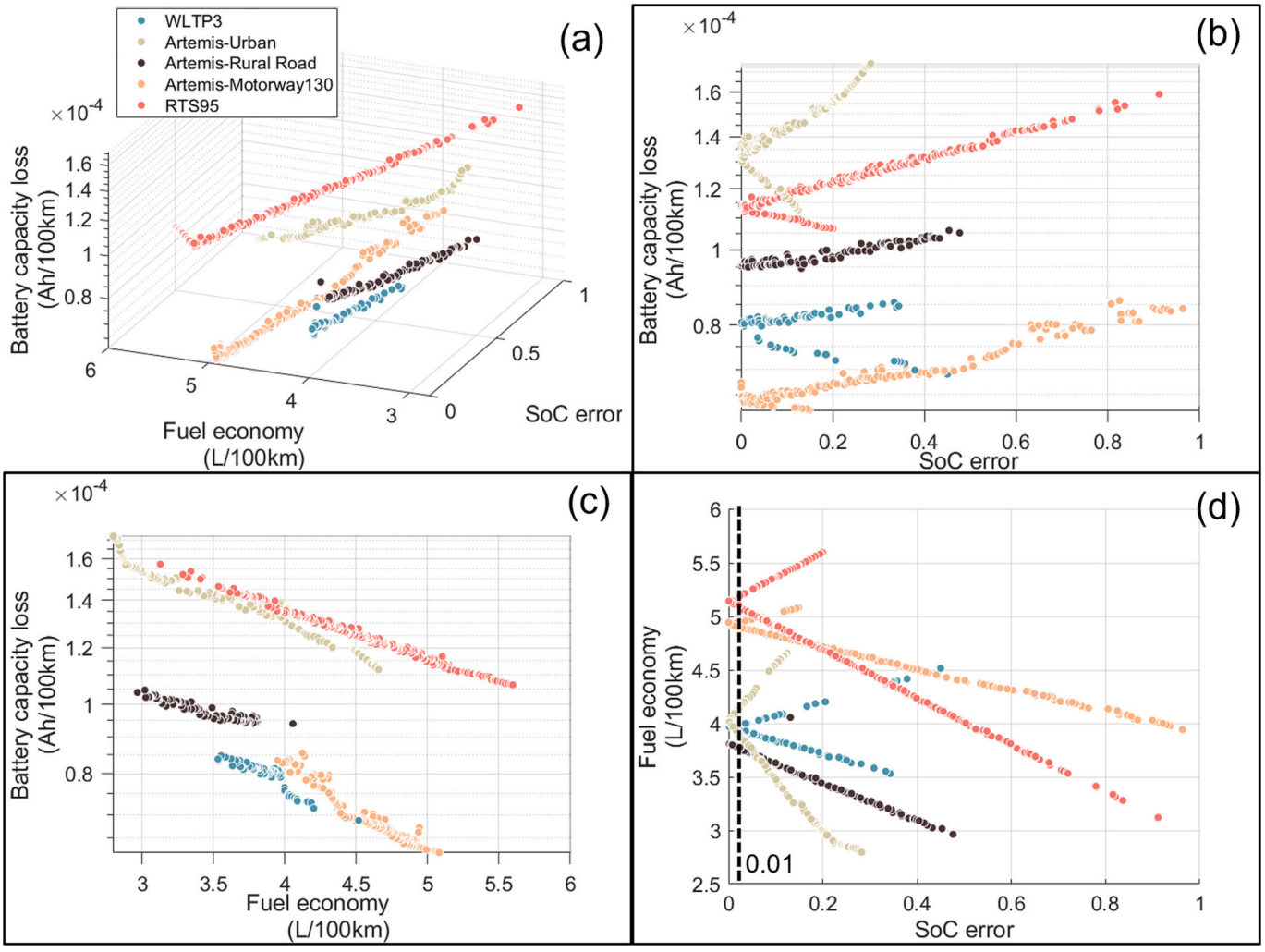

Fig. 6. Pareto frontier in five cycles. (a) PF in 3D space. (b) Projection on Fuel economy-Battery capacity loss coordinates. (c) Projection on SoC error-Battery capacity loss coordinates. (d) Projection on SoC error-Fuel economy coordinates.

mitigation into neither fuel-saving control nor SoC sustaining control as in the previous research [37,43,52].

Determining unified settings for EF and AF is important for the practice since the settings should be fixed for real-time control that offer a high level of robustness. This paper introduced a Pareto method to determine the global optimal EF and AF setting based on the Pareto Frontiers obtained in Fig. 6. By collecting the respective EF and AF values that formulate the Pareto Frontiers in Fig. 7, the unified EF and AF settings (EF = 1.40 and AF = 1.30) can be found by choosing the nearest neighborhood values of the average EF and AF values (illustrated by the two red dash lines in Fig. 7). For the rest of this paper, the C-ECMS method with the unified settings is named as C-ECMS-U, where the capital letter U represents 'unified'.

5.3. Evaluation of controlled results with baseline methods

To demonstrate the effectiveness of the proposed C-ECMS, a comparative study is conducted under five standard driving cycles to evaluate the vehicle performance, including fuel economy, SoC sustaining accuracy, and battery capacity loss. The C-ECMS methods with two types of parameter settings for EF and AF are studied, i.e., 1) C-ECMS-U with a unified setting (determined in 5.2) and 2) C-ECMS-I with independent parameter settings optimized for each cycle. The Rule-based control strategy, the standard ECMS and an offline DP computation are used as the baseline methods. Detailed settings for C-ECMS methods and baseline methods are illustrated in Table 3. Since the PHEV's operation in charging-depleting (CD) stages is similar to the pure EV, this paper mainly focuses on the charging-sustaining (CS) stage with an initial battery SoC of 0.3.

The vehicle performances under all five studied driving cycles are compared in Table 4. The error of the SoC sustaining error (%), the fuel economy (L/100 km), and the battery capacity loss (Ah/100 km) of the PHEV are compared, and the relative improvements achieved by C-ECMS-U and C-ECMS-I are calculated.

In general, the proposed C-ECMS achieves significant improvements in SoC sustaining accuracy, fuel economy, and battery capacity loss mitigation compared to the RB method. On average, the C-ECMS-I leads to an SoC sustaining error of 0.4%, reduces fuel consumption by 8.4%, and battery capacity loss by 10.4%, compared to the standard ECMS method. Although the improvement in battery sustaining accuracy is not significant when compared with the standard ECMS in high-speed driving conditions (the Artemis Motorway 130 cycle and the RTS95 cycle), the C-ECMS-I still can reduce up to 7.1% fuel consumption and 16.7% battery capacity loss, e.g., under the Artemis urban cycles. This is because the proposed mechanism is capable of balancing long-term and short-term goals if the parameters are well-tuned.

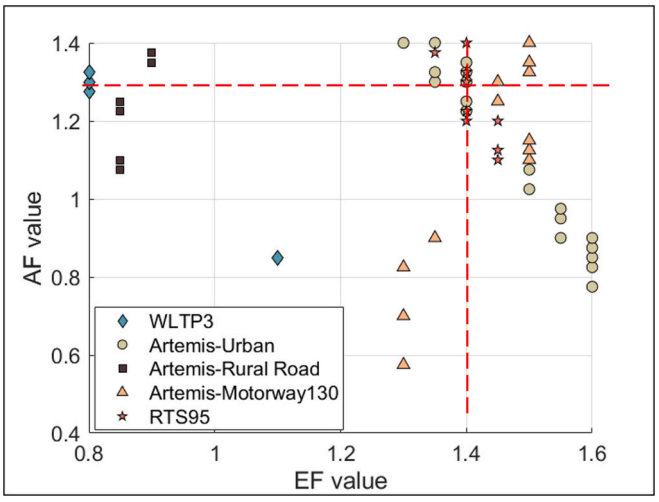

Fig. 7. The EF and AF distribution of Pareto frontiers for five cycles.

The DP results demonstrated the powertrain's theoretical optimal performance with the assumption that all road information was known beforehand. From the results summarized in Table 4, the PHEV controlled by the proposed C-ECMS-I is the closest to the benchmark results achieved by DP, followed by the C-ECMS-U. Both C-ECMS methods have gained many improvements over the rule-based method and the standard ECMS method.

Additionally, the results demonstrate that the proposed C-ECMS-U with the unified setting adapts well to most driving cycles and outperforms the rule-based method and the standard ECMS. While in some cases, the C-ECMS-U may fall short in achieving the best SoC (State of Charge) sustaining accuracy compared to the standard ECMS, this sacrifice is deemed acceptable in most driving cycles, as it aligns with the SAE standard.

For enhanced PHEV (Plug-in Hybrid Electric Vehicle) performance, optimizing the EF (Engine Factor) and AF (Acceleration Factor) settings based on individual cycle characteristics proves crucial. This is precisely why the C-ECMS-I method consistently outperforms other approaches, utilizing dedicated EF and AF settings.

5.4. Processor-in-the-loop (PiL) validation

The PiL testing platform used for control function verification is illustrated in Fig. 8. The PiL platform is based on ETAS LABCAR, a real-time computer with CAN interfaces and multiple I/Os. The vehicle model was downloaded from a host PC to the LABCAR through an Ethernet connection. The host PC is set based on a Windows 10 64-bit system with a CPU of 11th Gen Intel Core i7-11850H @ 2.50GHz, 16 GB RAM, and a graphic processor of NVIDIA GeForce GTX 3070. The energy management algorithms were subsequently complied with C code and implemented in the LABCAR's controller for real-time validation. The controller and the vehicle plant model were linked via CAN so that the LABCAR could emulate the CAN-based communication in the car. The data was exchanged in real time between the controller and the vehicle plant model in the PiL test, and a data file was recorded for vehicle performance evaluation. During the real-time control, the maximum memory used by the control algorithm is 78 kb, and the control calculation requires 0.06 s for each time step of 1 s.

The PiL results of the PHEV controlled by the RB method, standard ECMS, and C-ECMS under the WLTP3 cycle are compared with DP offline simulation results in Fig. 9. The C-ECMS implements an EF and AF setting that is optimized for WLTP3 cycle. All four approaches control the final SoC close to the target sustaining level as illustrated in Fig. 9 (b). Fig. 9 (c) demonstrates that the C-ECMS can significantly improve the fuel economy by achieving less fuel consumption per 100 km with a value of 3.880 $L/100km$, which is closed to the DP results (3.840 $L/100km$), and it is 15.5% less than RB methods (4.592 $L/100km$) and 13.9% (4.506 $L/100km$) less than conventional ECMS. Fig. 9(e) and (f) show that the C-ECMS allocates MG2 with lower torque commands in the high-speed idle areas and attributes higher torque compensations to the ICE than the other baseline methods. Fig. 9(d) shows that the proposed C-ECMS can reduce battery capacity loss by 21.5% and 22.9% compared to the RB method and standard ECMS, respectively. From Fig. 9, the powertrain controlled by C-ECMS exhibits a different SoC trend, with a discharge-before-charge pattern compared to the conventional method at the time of the 1500s, 3250 s, and 5000 s. This is because the C-ECMS has a better sense of control to prevent battery degradation. Remaining discharging the battery to drive MG2 during these periods will help mitigate battery capacity degradation compared to frequently charging and discharging. This resulted in lower battery capacity loss with the proposed C-ECMS compared to other methods as illustrated in Fig. 9(d).

Table 3
Parameter settings for comparative methods.

Control Strategy	Working status		Working conditions	Setup		
				Initial SoC	Discretization	EF and AF
Rule-based	Hybrid mode switching		CS	0.3	None	None
Standard ECMS	Power distribution	MG1, ICE	CS	0.3	$m = 30$	Only EF considered
C-ECMS-U	Power distribution	MG1, MG2, ICE	CS	0.3	$n = m = 30$	Unified parameters
C-ECMS-I	Power distribution	MG1, MG2, ICE	CS	0.3	$n = m = 30$	Independent parameters
Dynamic programming	Offline optimal calculation	CS	0.3	$n = m = 30$	None	

Table 4
Comparison of C-ECMS with baseline methods.*

Driving cycle	Methods	SoC error	Fuel economy ($L/100km$)	Fuel consumption reduction of the standard ECMS	Battery capacity loss ($10^{-5}Ah/100km$)	Battery capacity loss reduction of the standard ECMS
WLTP3	Rule-based	6.3%	4.608	–	10.122	–
	ECMS	2.1%	4.508	–	10.298	–
	C-ECMS-U	2.3%	4.535	−0.6%	7.130	30.8%
	C-ECMS-I	0.3%	3.860	12.0%	7.959	22.7%
	DP	0.0%	3.840	–	7.779	–
Artemis Urban	Rule-based	1.0%	4.493	–	21.513	–
	ECMS	0.6%	4.570	–	19.265	–
	C-ECMS-U	1.4%	4.245	7.1%	16.042	16.7%
	C-ECMS-I	0.6%	4.215	7.8%	16.039	16.7%
	DP	0.0%	4.206	–	15.983	–
Artemis Rural Road	Rule-based	6.3%	4.503	–	10.988	–
	ECMS	0.0%	4.173	–	11.065	–
	C-ECMS-U	7.5%	4.147	0.6%	9.440	14.7%
	C-ECMS-I	0.5%	3.804	8.8%	9.504	14.1%
	DP	0.0%	3.708	–	9.487	–
Artemis Motorway 130	Rule-based	2.8%	5.267	–	6.728	–
	ECMS	1.6%	5.168	–	6.083	–
	C-ECMS-U	1.0%	4.920	4.8%	6.582	−8.2%
	C-ECMS-I	0.3%	4.927	4.7%	6.474	−6.4%
	DP	0.0%	4.905	–	4.213	–
RTS95	Rule-based	3.3%	5.814	–	12.378	–
	ECMS	0.2%	5.621	–	11.903	–
	C-ECMS-U	0.4%	5.128	8.8%	11.210	5.8%
	C-ECMS-I	0.5%	5.137	8.6%	11.344	4.7%
	DP	0.0%	5.082	–	10.093	–
Average values of C-ECMS-I**		0.4%	–	8.4%	–	10.4%

* The values are calculated based on the results of the standard ECMS.
** Average value is calculated based on the five driving cycles.

6. Conclusion

This paper proposes a Cuboid Equivalent Consumption Minimization Strategy (C-ECMS) for multimode PHEVs. Experiments under five driving cycles are conducted to study 1) the impact of Hamiltonian matrix dimensions on SoC control accuracy and 2) the impact of EF and AF settings on the Pareto Frontier considering fuel economy, SoC accuracy, and battery aging. The C-ECMS-U with a unified setting obtained by the numerical analysis and the C-ECMS-I with independent settings from Pareto frontier analysis of cycles are compared with the rule-based strategy and the standard ECMS implemented in the same PHEV. The conclusions drawn from the investigation are as follows.

1) The orthogonal experiment on the numbers of elements in the Hamiltonian matrix indicates that the Hamiltonian matrix with a size of 30-by-30 is the best when considering SoC sustaining accuracy and computational effort.
2) Based on 5×5600 groups of individual testing with different combinations of AF and EF, the unified AF and EF settings are obtained using Pareto Frontier analysis. It is suggested that the studied PHEV can be adapted to most driving conditions with the unified setting fixed for real-time control.
3) By introducing the aging factor (AF), the C-ECMS-U using the unified setting is adaptive to most driving cycles and performs better than the rule-based method and the standard ECMS. The C-ECMS-U performs accordingly to the driving cycles. Specifically in the Artemis Urban cycle, up to 7.1% of the fuel consumption can be saved and 16.7% of the battery capacity loss can be mitigated from the standard ECMS method.

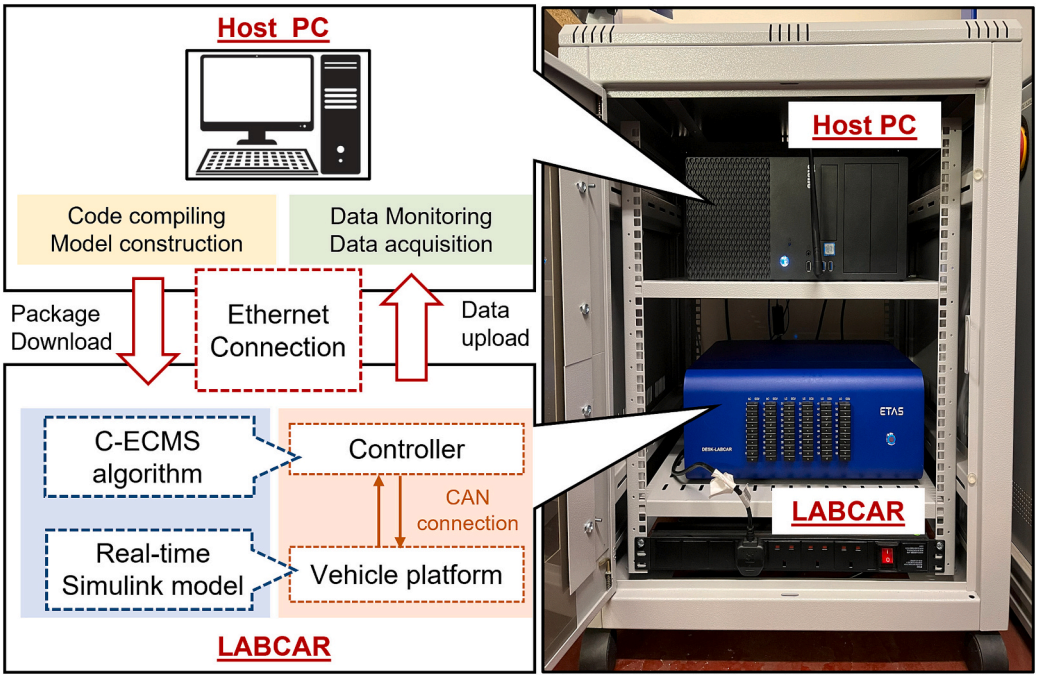

Fig. 8. The PiL test platform.

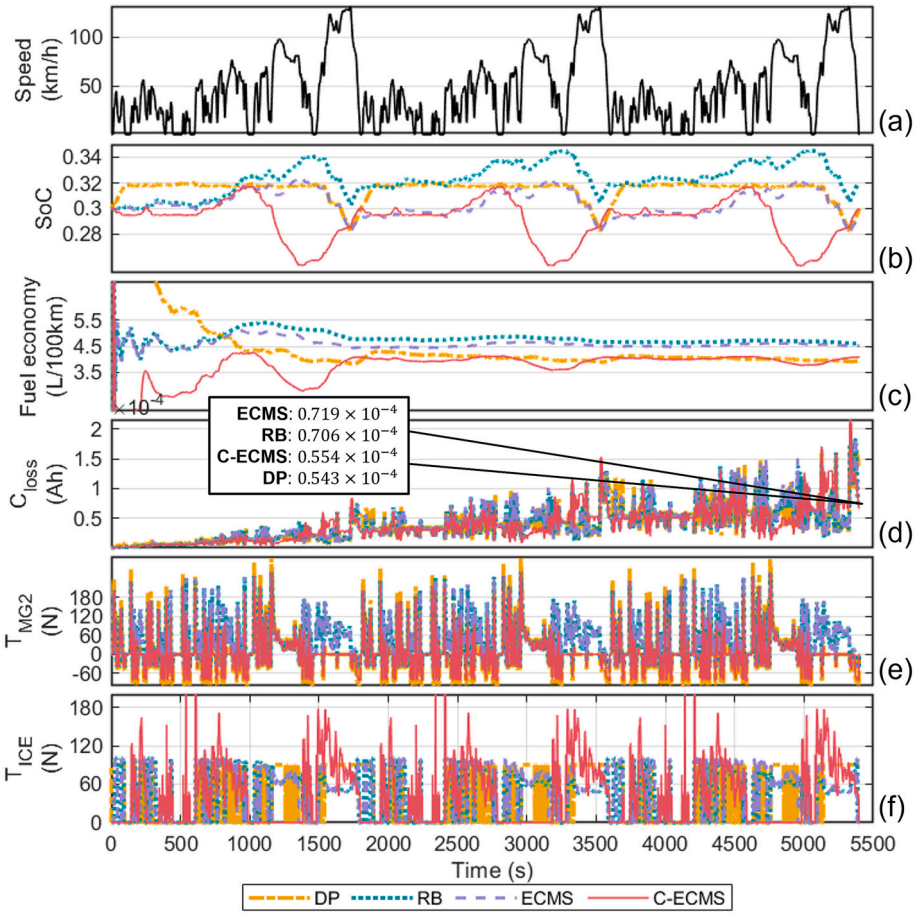

Fig. 9. Comparison of PHEV's performances based on three control strategy and DP offline simulation. (a) Test driving cycle. (b) SoC variations. (c) Fuel economies of the PHEV. (d) Battery capacity losses. (e) Torque generated by MG2. (f) Torque generated by ICE.

4) The C-CEMS-I can control both motors' actions based on the Hamiltonian matrices and achieves the best performance in terms of SoC sustaining accuracy, fuel economy, and battery capacity loss compared to the RB method and the standard ECMS. On average, it conducts an SoC sustaining error of 0.4%, fuel consumption by 8.4%, and battery capacity loss by 10.4%, compared to the standard ECMS method.

CRediT authorship contribution statement

Cetengfei Zhang: Writing – original draft, Validation, Methodology, Investigation, Conceptualization. **Quan Zhou:** Writing – review & editing, Supervision, Conceptualization. **Min Hua:** Validation, Software, Methodology. **Hongming Xu:** Writing – review & editing, Supervision, Project administration. **Mike Bassett:** Writing – review & editing, Methodology, Conceptualization.

Declaration of Competing Interest

The authors declares no potential competing interests.

Data availability

Data will be made available on request.

References

[1] Nallusamy N, Sakthivel P, Chausalkar A, Ramadhas AS. Electric vehicles Setting a course for 2030. Alternat Fuels for Transportat 2020:295–320.
[2] I. World Energy Outlook 2020, Paris, 2020 [Online]. Available: https://www.iea.org/reports/world-energy-outlook-2020; 2020.
[3] Silvas E, Hofman T, Murgovski N, Etman LFP, Steinbuch M. Review of optimization strategies for system-level design in hybrid electric vehicles. IEEE Trans Veh Technol 2016;66(1):57–70. https://doi.org/10.1109/TVT.2016.2547897.
[4] Huang Y, et al. A review of power management strategies and component sizing methods for hybrid vehicles. Renew Sust Energ Rev 2018;96(August):132–44. https://doi.org/10.1016/j.rser.2018.07.020.
[5] Hua M, Chen G, Zhang B, Huang Y. A hierarchical energy efficiency optimization control strategy for distributed drive electric vehicles. Proc Inst Mech Eng Part D J Automob Eng 2019;233(3):605–21. https://doi.org/10.1177/0954407017751788.
[6] Zhou Q, Zhang Y, Li Z, Li J, Xu H, Olatunbosun O. Cyber-physical energy-saving control for hybrid aircraft-towing tractor based on online swarm intelligent programming. IEEE Trans Ind Informat 2018;14(9):4149–58. https://doi.org/10.1109/TII.2017.2781230.
[7] Zhou Q, Zhang W, Cash S, Olatunbosun O, Xu H, Lu G. Intelligent sizing of a series hybrid electric power-train system based on Chaos-enhanced accelerated particle swarm optimization. Appl Energy 2017;189:588–601. https://doi.org/10.1016/j.apenergy.2016.12.074.
[8] Zhou Q, et al. Multi-step reinforcement learning for model-free predictive energy management of an electrified off-highway vehicle. Appl Energy 2019;255(June). https://doi.org/10.1016/j.apenergy.2019.113755.
[9] Paganelli G, Delprat S, Guerra TM, Rimaux J, Santin JJ. Equivalent consumption minimization strategy for parallel hybrid powertrains. IEEE Veh Technol Conf 2002;4:2076–81. https://doi.org/10.1109/VTC.2002.1002989.
[10] Chen Z, Liu Y, Ye M, Zhang Y, Li G. A survey on key techniques and development perspectives of equivalent consumption minimisation strategy for hybrid electric vehicles. Renew Sust Energ Rev 2020;151(November):2021. https://doi.org/10.1016/j.rser.2021.111607.
[11] Onori S. Hybrid electric vehicles energy management strategies. 2016.
[12] Li J, Liu Y, Qin D, Li G, Chen Z. Research on equivalent factor boundary of equivalent consumption minimization strategy for PHEVs. IEEE Trans Veh Technol 2020;69(6):6011–24. https://doi.org/10.1109/TVT.2020.2986541.
[13] Choi K, Byun J, Lee S, Jang IG. Adaptive equivalent consumption minimization strategy (A-ECMS) for the HEVs with a near-optimal equivalent factor considering driving conditions. IEEE Trans Veh Technol 2022;71(3):2538–49. https://doi.org/10.1109/TVT.2021.3127691.
[14] Hegde S, Bonfitto A, Rahmeh H, Amati N, Tonoli A. Optimal selection of equivalence factors for ECMS in mild hybrid electric vehicles. Proc ASME Des Eng Tech Conf 2021;1:1–9. https://doi.org/10.1115/DETC2021-71621.
[15] Sun C, Sun F, He H. Investigating adaptive-ECMS with velocity forecast ability for hybrid electric vehicles. Appl Energy 2017;185:1644–53. https://doi.org/10.1016/j.apenergy.2016.02.026.
[16] Xie S, Hu X, Qi S, Lang K. An artificial neural network-enhanced energy management strategy for plug-in hybrid electric vehicles. Energy 2018;163:837–48. https://doi.org/10.1016/j.energy.2018.08.139.
[17] Brunelli L, et al. A predictive control strategy based on A-ECMS to handle zero-emission zones: performance assessment and testing using an HiL equipped with vehicular connectivity. Appl Energy 2023;340(January). https://doi.org/10.1016/j.apenergy.2023.121008.
[18] Zhang Y, et al. An improved adaptive equivalent consumption minimization strategy for parallel plug-in hybrid electric vehicle. Proc Inst Mech Eng Part D J Automob Eng 2019;233(6):1649–63. https://doi.org/10.1177/0954407018805605.
[19] Bouwman KR, Pham TH, Wilkins S, Hofman T. Predictive energy management strategy including traffic flow data for hybrid electric vehicles. In: IFAC-PapersOnLine. 50; 2022. p. 10046–51. https://doi.org/10.1016/j.ifacol.2017.08.1775. no. 1.
[20] Zhang X, Yang L, Sun X, Jin Z, Xue M. ECMS-MPC energy management strategy for plug-in hybrid electric buses considering motor temperature rise effect. IEEE Trans Transp Electrif 2023;9(1):210–21. https://doi.org/10.1109/TTE.2022.3195945.
[21] Li X, Wang Z, Yan J. Prognostic health condition for lithium battery using the partial incremental capacity and Gaussian process regression. J Power Sources 2019;421(January):56–67. https://doi.org/10.1016/j.jpowsour.2019.03.008.
[22] Han X, Ouyang M, Lu L, Li J, Zheng Y, Li Z. A comparative study of commercial lithium ion battery cycle life in electrical vehicle: aging mechanism identification. J Power Sources 2014;251:38–54. https://doi.org/10.1016/j.jpowsour.2013.11.029.
[23] Lin Q, Wang J, Xiong R, Shen W, He H. Towards a smarter battery management system: a critical review on optimal charging methods of lithium ion batteries. Energy 2019;183:220–34. https://doi.org/10.1016/j.energy.2019.06.128.
[24] Han X, et al. A review on the key issues of the lithium ion battery degradation among the whole life cycle. eTransportation 2019;1:100005. https://doi.org/10.1016/j.etran.2019.100005.
[25] Li Y, Stroe D, Cheng Y, Sheng H, Sui X. On the feature selection for battery state of health estimation based on charging – discharging profiles. J Energy Stor 2021;33(September):102122. https://doi.org/10.1016/j.est.2020.102122. 2020.
[26] Verma P, Maire P, Novák P. A review of the features and analyses of the solid electrolyte interphase in Li-ion batteries. Electrochim Acta 2010;55(22):6332–41. https://doi.org/10.1016/j.electacta.2010.05.072.
[27] Crawford AJ, Choi D, Balducci PJ, Subramanian VR, Viswanathan VV. Lithium-ion battery physics and statistics-based state of health model. J Power Sources 2021;501(April):230032. https://doi.org/10.1016/j.jpowsour.2021.230032.
[28] Galeotti M, Cinà L, Giammanco C, Cordiner S, Di Carlo A. Performance analysis and SOH (state of health) evaluation of lithium polymer batteries through electrochemical impedance spectroscopy. Energy 2015;89:678–86. https://doi.org/10.1016/j.energy.2015.05.148.
[29] Liu W, Placke T, Chau KT. Overview of batteries and battery management for electric vehicles. Energy Rep 2022;8:4058–84. https://doi.org/10.1016/j.egyr.2022.03.016.
[30] Li P, et al. State-of-health estimation and remaining useful life prediction for the lithium-ion battery based on a variant long short term memory neural network. J Power Sources 2020;459(October 2019):228069. https://doi.org/10.1016/j.jpowsour.2020.228069.
[31] Tian J, Xiong R, Shen W, Lu J. State-of-charge estimation of LiFePO4 batteries in electric vehicles: a deep-learning enabled approach. Appl Energy 2021;291(5):116812. https://doi.org/10.1016/j.apenergy.2021.116812.
[32] Li Y, et al. Data-driven health estimation and lifetime prediction of lithium-ion batteries: a review. Renew Sust Energ Rev 2019;113(July). https://doi.org/10.1016/j.rser.2019.109254.
[33] Xiong R, Zhang Y, Wang J, He H, Peng S, Pecht M. Lithium-ion battery health prognosis based on a real battery management system used in electric vehicles. IEEE Trans Veh Technol 2019;68(5):4110–21. https://doi.org/10.1109/TVT.2018.2864688.
[34] Pelletier S, Jabali O, Laporte G, Veneroni M. Battery degradation and behaviour for electric vehicles: review and numerical analyses of several models. Transp Res Part B Methodol 2017;103:158–87. https://doi.org/10.1016/j.trb.2017.01.020.
[35] Suri G, Onori S. A control-oriented cycle-life model for hybrid electric vehicle lithium- ion batteries. Energy 2016;96:644–53. https://doi.org/10.1016/j.energy.2015.11.075.
[36] Wang J, et al. Cycle-life model for graphite-LiFePO4 cells. J Power Sources 2011;196(8):3942–8. https://doi.org/10.1016/j.jpowsour.2010.11.134.
[37] Tang L, Rizzoni G, Onori S. Energy management strategy for HEVs including battery life optimization. IEEE Trans Transp Electrif 2015;1(3):211–22. https://doi.org/10.1109/TTE.2015.2471180.
[38] Xiong R, Pan Y, Shen W, Li H, Sun F. Lithium-ion battery aging mechanisms and diagnosis method for automotive applications: recent advances and perspectives. Renew Sust Energ Rev 2020;131(5):110048. https://doi.org/10.1016/j.rser.2020.110048.
[39] Hu X, et al. Multiobjective optimal sizing of hybrid energy storage system for electric vehicles 2018;67(2):1027–35.
[40] Song Z, Hofmann H, Li J, Hou J, Han X, Ouyang M. Energy management strategies comparison for electric vehicles with hybrid energy storage system. Appl Energy 2014;134:321–31. https://doi.org/10.1016/j.apenergy.2014.08.035.
[41] Musardo C, Rizzoni G, Guezennec Y, Staccia B. A-ECMS: an adaptive algorithm for hybrid electric vehicle energy management. Eur J Control 2005;11(4–5):509–24. https://doi.org/10.3166/ejc.11.509-524.
[42] Liang Y. PHEV hybrid vehicle system efficiency and battery aging optimization using A-ECMS based algorithms. 2020. p. 1–9. https://doi.org/10.4271/2020-01-1178.Abstract.
[43] Sarvaiya S, Ganesh S, Xu B. Comparative analysis of hybrid vehicle energy management strategies with optimization of fuel economy and battery life. Energy 2021;228:120604. https://doi.org/10.1016/j.energy.2021.120604.

[44] Hu X, Li S, Peng H. A comparative study of equivalent circuit models for Li-ion batteries 2012;198:359–67. https://doi.org/10.1016/j.jpowsour.2011.10.013.
[45] Zhou S, Liu X, Hua Y, Zhou X, Yang S. Adaptive model parameter identification for lithium-ion batteries based on improved coupling hybrid adaptive particle swarm optimization- simulated annealing method. J Power Sources 2021;482(September 2020):228951. https://doi.org/10.1016/j.jpowsour.2020.228951.
[46] Hu Z, et al. Multi-objective energy management optimization and parameter sizing for proton exchange membrane hybrid fuel cell vehicles. Energy Convers Manag 2016;129:108–21. https://doi.org/10.1016/j.enconman.2016.09.082.
[47] Song Z, et al. Multi-objective optimization of a semi-active battery/supercapacitor energy storage system for electric vehicles. Appl Energy 2014;135:212–24. https://doi.org/10.1016/j.apenergy.2014.06.087.
[48] Song Z, Hofmann H, Li J, Han X, Zhang X, Ouyang M. A comparison study of different semi-active hybrid energy storage system topologies for electric vehicles. J Power Sources 2015;274:400–11. https://doi.org/10.1016/j.jpowsour.2014.10.061.
[49] The Engineering ToolBox. Fuels - higher and lower calorific values. 2003. p. 2003. https://www.engineeringtoolbox.com/fuels-higher-calorific-values-d_169.html.
[51] Buchmann Isidor. Battery university: safety of lithium-ion batteries. https://batteryuniversity.com/article/safety-of-lithium-ion-batteries; 2017.
[52] Serrao L, Onori S, Sciarretta A, Guezennec Y, Rizzoni G. Optimal energy management of hybrid electric vehicles including battery aging. Proc Am Control Conf 2011;3:2125–30. https://doi.org/10.1109/acc.2011.5991576.